Virologica Sinica 40 (2025) 735–747

Contents lists available at ScienceDirect

Virologica Sinica

journal homepage: www.keaipublishing.com/en/journals/virologica-sinica
www.virosin.org

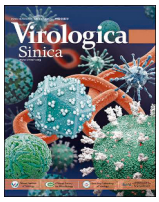

Research Article

Phylogenomics and structural modelling feature accelerated evolution of Oropouche virus: 1955 to 2024

Yibo Ding [a], Jiajing Li [b], Xin Wang [b], Simone Malagò [c,d], Amaro Nunes Duarte-Neto [e], Xiaohui Ding [a], Fang Qin [a], Michela Deiana [d], Concetta Castilletti [d], Hongbo Guo [a,*], Qiuwei Pan [b,*], Wenshi Wang [a,*]

[a] Department of Pathogen Biology and Immunology, Jiangsu Key Laboratory of Immunity and Metabolism, Jiangsu International Laboratory of Immunity and Metabolism, Xuzhou Medical University, Xuzhou, 221004, China
[b] Department of Gastroenterology and Hepatology, Erasmus MC-University Medical Center, Rotterdam, 3015 GD, the Netherlands
[c] PhD National Programme in One Health Approaches to Infectious Diseases and Life Science Research, Department of Public Health, Experimental and Forensic Medicine, University of Pavia, Pavia, 27100, Italy
[d] Department of Infectious-Tropical Diseases and Microbiology, IRCCS Sacro Cuore Don Calabria Hospital, Negrar di Valpolicella, Verona, 37024, Italy
[e] Departamento de Patologia, Faculdade de Medicina, Universidade de São Paulo, São Paulo, 05508-000, Brazil

ARTICLE INFO

Keywords:
Oropouche virus (OROV)
Phylogenomic analysis
Spatiotemporal evolution
Protein structure
Reassortment

ABSTRACT

A large multi-country outbreak of Oropouche virus (OROV), a segmented negative-sense RNA virus, is emerging in Latin America. By analyzing publicly available whole-genome sequences spanning 1955 to 2024, this study reveals accelerated spatiotemporal evolution of OROV, cooperatively driven by genome mutagenesis and segment reassortment. The strains responsible for the 2023–2024 outbreak are universally reassortants, but form two divergent lineages, namely the Brazil and western Amazon basin lineages. This epidemic spreading is primarily fueled by localized transmission within countries and cross-border spread. Phylogenomic analysis further suggests that the S segment of the viral genome originated in Brazil around the 1740s, underwent diversification into five distinct clusters by the 1970s, and experienced rapid proliferation during 2020–2024. In contrast, the L segment originated in Peru around the 1630s and evolved into two independent clusters by the 1850s. Divergent evolutionary pressures have driven distinct patterns of amino acid changes in viral proteins between the Brazil and the western Amazon basin lineages. These mutations are predicted to alter the protein structures and bear functional consequences for viral fitness and transmission. These findings provide critical insights into the evolutionary dynamics of OROV and underscore the necessity of genome surveillance to track the transmission pathways and spatiotemporal evolution.

INTRODUCTION

The Oropouche virus (OROV) is an arbovirus transmitted primarily by biting midges. The virus was first identified in 1955 in the village of Oropouche, located in Trinidad and Tobago (Anderson et al., 1961). Although OROV was traditionally endemic in the Amazon region, the current 2023–2024 outbreak is rapidly expanding beyond the usual endemic region and reaching densely populated urban areas. By October 2024, over 10,000 confirmed cases have been reported in Latin America, in countries including Brazil, Peru, Bolivia, Colombia, Guyana and Cuba (Anderer, 2024; Pan American Health Organization, 2024; Tilston-Lunel, 2024). Additionally, travel-imported cases have been recorded in the United States, Canada and European countries (Baer et al., 2024; Capobianchi et al., 2024; Castilletti et al., 2024; Deiana et al., 2024; Guagliardo et al., 2024; Lenharo, 2024). Like other arboviruses (Harris et al., 2019; Nakase et al., 2023), the OROV outbreak is thought to be associated with climate change, human mobility, specific agricultural production (Graf et al., 2024; Iani et al., 2024).

OROV is a single-stranded, negative-sense RNA virus of the family *Peribunyaviridae*, genus *Orthobunyavirus*, species *Orthobunyavirus*

* Corresponding authors.
E-mail addresses: wenshi.wang@xzhmu.edu.cn (W. Wang), q.pan@erasmusmc.nl (Q. Pan), hongbo.guo@xzhmu.edu.cn (H. Guo).

https://doi.org/10.1016/j.virs.2025.09.009
Received 12 May 2025; Accepted 28 September 2025
Available online 2 October 2025

oropoucheense, with the genome contains three individual segments: the small (S), medium (M) and large (L) segments. The S segment encodes nucleocapsid and a non-structural protein (NSs), the M segment encodes two glycoproteins and a non-structural protein (NSm), and the L segment encodes RNA-dependent RNA polymerase (RdRp) (Elliott, 2014; Travassos Da Rosa et al., 2017). As an RNA virus, OROV has an extremely high rate of mutagenesis, attributed to the RdRp's lack of proofreading machinery. In addition, the segmented OROV genome could enhance the likelihood of reassortment events (Elliott, 2014; Gutierrez et al., 2020). It has been reported that the upsurge of OROV cases in the Brazilian Amazon from 2022 to 2024 coincides with the spread of a novel reassortant lineage containing the M segment of viruses detected in the eastern Amazon region (2009–2018) and the L and S segments of viruses detected in Peru, Colombia, and Ecuador (2008–2021) (Naveca et al., 2024). Additionally, the current outbreak has uniquely spanned at least two consecutive rainy seasons, further complicating its dynamics (Naveca et al., 2024). Interestingly, in cell culture models, it has been shown that the 2023–2024 epidemic isolate (AM0088) exhibits significantly higher replication efficiency than the historical prototype strain (BeAn19991) isolated from the 1960s (Scachetti et al., 2024). Collectively, these findings suggest that OROV may be undergoing evolutionary adaptations, resulting in increased transmission efficiency and potentially more severe disease outcomes (Scachetti et al., 2024).

Oropouche fever, caused by OROV, was previously thought to be generally mild and self-limiting. However, during the 2023–2024 outbreak, severe OROV-associated complications have been reported, including vertical transmission, stillbirth, newborns with microcephaly, as well as fatalities in otherwise healthy young adults (Lenharo, 2024; Martins-Filho et al., 2024; Moutinho, 2024). This prompted us to systematically investigate the genetic landscapes of OROV from 1955 to 2024, for better understanding the mysterious changes in its epidemiological, clinical features, as well as viral adaptation. Herein, we retrieved all publicly available OROV sequences to analyze the landscape of OROV transmission and spatiotemporal evolution. Furthermore, we characterized the impact genomic mutations on amino acid and protein structural changes.

RESULTS

Phylogenomic analysis captures temporal evolution of OROV

To characterize the phylogenomics of OROV, we retrieved 2147 sequences (701 L, 715 M, and 731 S segments) of species *Orthobunyavirus oropoucheense* from 1955 to 2024 (accessed on October 10th, 2024) (Fig. 1). After rigorous screening, 524 strains with complete genome sequences (L, M, S segments) were included (Fig. 1, dataset A, B, and C). These consist of 518 OROV, two Iquitos virus (IQTV) (Aguilar et al., 2011), two Madre de Dios virus (MDDV) (Navarro et al., 2016), and two Perdões virus (PDEV) (Tilston-Lunel et al., 2015) strains (Supplementary Table S1–S3). Among these strains, 481 were from Brazil, 18 from Peru, 10 from Colombia, 1 from Trinidad and Tobago (Anderson et al., 1961), 1 from French Guiana (Gaillet et al., 2021), 1 from Haiti (Elbadry et al., 2021), 4 from Panama, 6 from Ecuador 1 from Venezuela, and 1 from Italy (Supplementary Table S1–S3).

Phylogenetic trees were constructed for each of the three segments (dataset A, B, and C, Fig. 2A–C, and Supplementary Fig. S1-S3). The analyses revealed distinct clustering patterns for each segment. For the L segment, two clusters emerged between 1955 and 2024 (Fig. 2A, and Supplementary Fig. S1). Cluster L_I comprised the earliest OROV isolate, TRVL9760 (from Trinidad and Tobago, 1955) (Acrani et al., 2015), alongside strains isolated from Brazil and Panama between 1960 and 2006 (Supplementary Fig. S1). Cluster L_{II} encompassed OROV strains isolated from Brazil, Peru, Colombia, Ecuador, Haiti, Italy, and French Guiana between 1991 and 2024, alongside IQTV, and PDEV (Supplementary Fig. S1). The M segment diverged into three clusters (1955–2024) (Supplementary Fig. S2). Cluster M_I included the earliest isolated OROV strain (TRVL9760), along with strains from Brazil and Panama collected between 1960 and 2006. Cluster M_{II} comprised strains isolated from Brazil, Peru, Haiti, French Guiana, and Italy from 2009 to

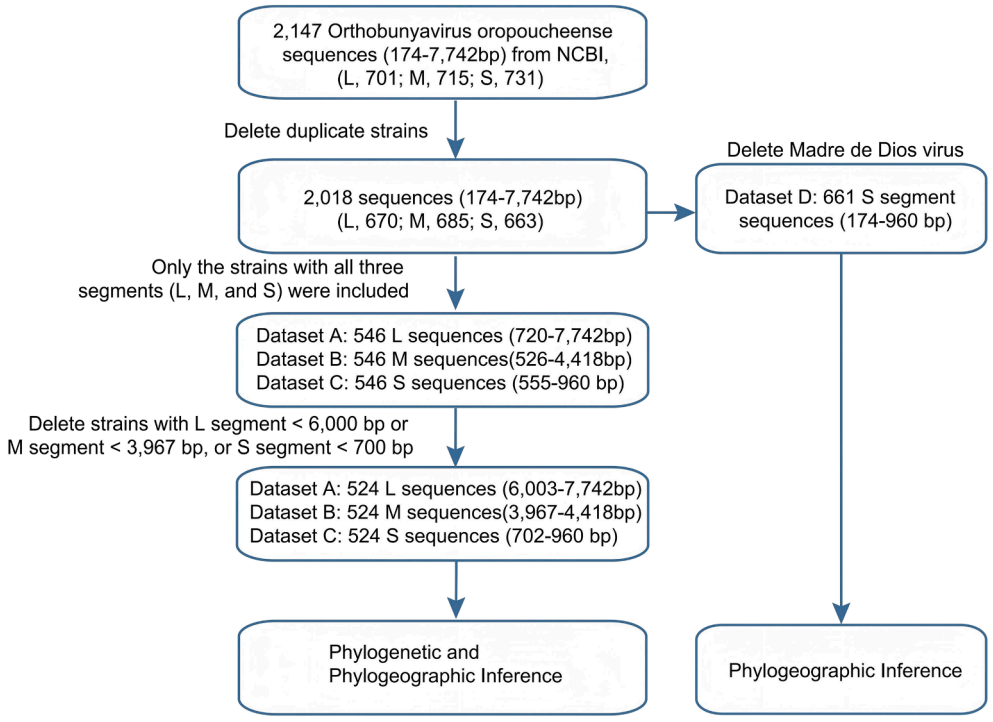

Fig. 1. Flowchart of the establishment of datasets used in this study. Flow diagram illustrating the establishment of datasets A, B, C, and D. After rigorous screening, 524 L, M, and S segment sequences were included in the dataset A, B and C, respectively. For the phylogeographic and sensitivity analyses, all available S segment sequences (661 sequences in total) were included in the dataset D.

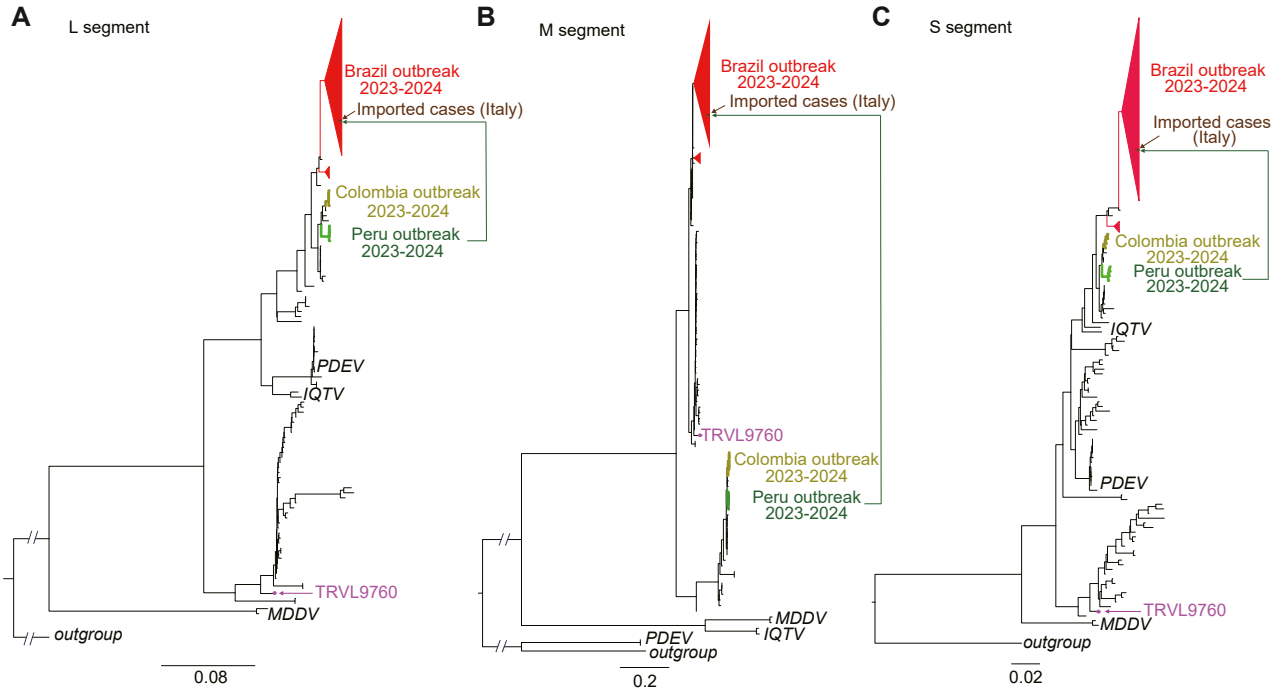

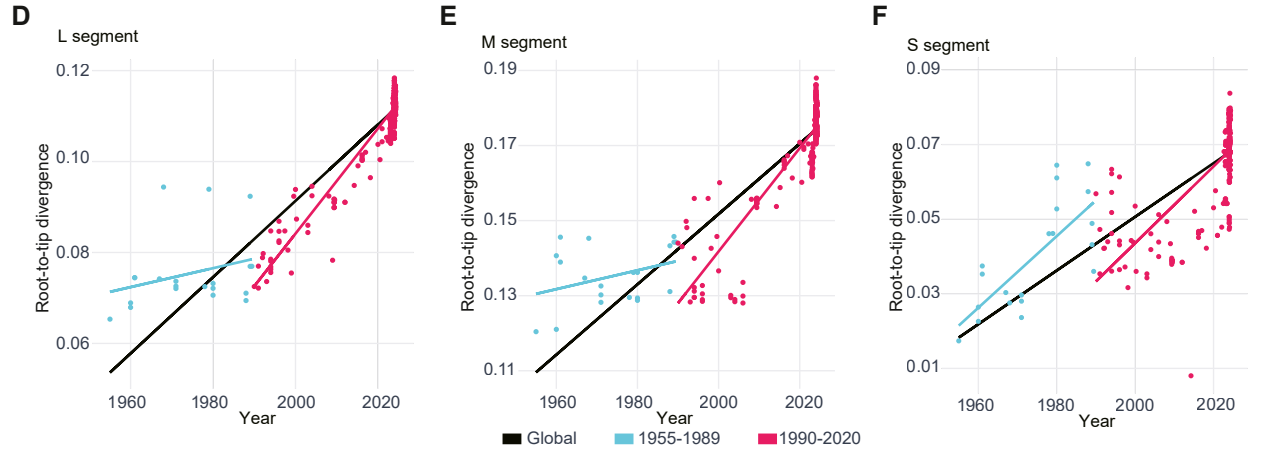

G

Root-to-tip (RTT) regression of L, M, and S genomes

		L			M			S		
	Nodes	Rate (substitution /site/year)	R^2	Residual Mean Squared	Rate (substitution /site/year)	R^2	Residual Mean Squared	Rate (substitution /site/year)	R^2	Residual Mean Squared
Global	524	8.39 E-4	0.85	1.80 E-5	6.90 E-4	0.80	3.80 E-5	7.19 E-4	0.54	8.40 E-5
1955-1989	20	2.08 E-4	0.10	6.76 E-5	2.08 E-4	0.10	5.93 E-5	9.60 E-4	0.55	2.61 E-4
1990-2024	504	1.16 E-3	0.87	0.87 E-5	9.89 E-4	0.83	2.46 E-5	1.03 E-3	0.49	6.47 E-5

ND: not determined

Fig. 2. Temporal dynamics of OROV. **A–C** Maximum-likelihood phylogenetic trees of the L (**A**), M (**B**), and S (**C**) segments based on datasets A, B, and C, respectively. The 2023–2024 outbreak-causing OROV sequences in the phylogenetic trees are highlighted in red (Brazil strains) and green (Peru strains). The first identified OROV strain (TRVL9760) was highlighted in purple. The 2024 OROV strain identified in Italy was highlighted in the color brown. The scale bar indicates the number of substitutions per site. Jatobal virus was used as an outgroup (Saeed et al., 2001). Iquitos virus, IQTV; Madre de Dios virus, MDDV; Perdões virus, PDEV. **D–G** The Clockor2 software was employed to infer global and local strict molecular clocks of the L segment (dataset A) (**D**), M segment (dataset B) (**E**), and S segment (dataset C) (**F**) by using the root-to-tip regression method. The evolutionary rates, and linear regression R-Squared were shown in (**G**).

2024. The strains isolated from Peru, Colombia, Ecuador, Brazil, and Panama from 1991 to 2024 formed cluster M_{III} (Supplementary Fig. S2). In contrast, the S segment formed five clusters (1955–2024) (Fig. 2C, and Supplementary Fig. S3). Cluster S_I included the earliest strain (TRVL9760), along with strains from Brazil, Haiti, and Panama collected between 1960 and 2004. Cluster S_{II} contained PDEV and OROV strains isolated from Brazil, Peru, and Panama from 1978 to 2018. A minor cluster, S_{III}, encompassed OROV strains isolated in Brazil between 1988 and 2000. Another minor cluster, S_{IV}, included two strains from Brazil isolated in 1980. The cluster S_V comprised OROV strains isolated from Brazil, Peru, Colombia, Ecuador, Haiti, Italy, and French Guiana between 1999 and 2024, alongside IQTV.

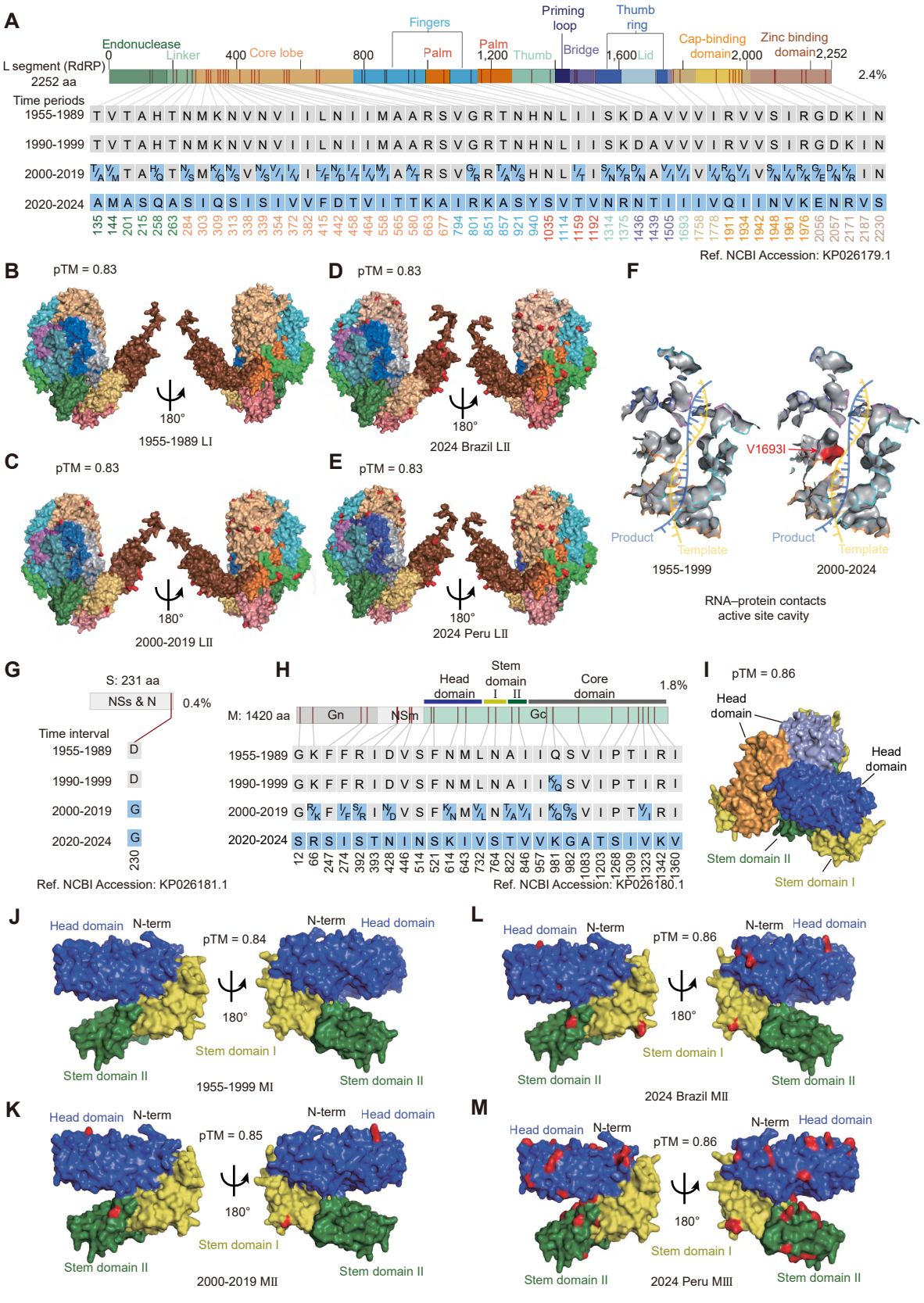

(caption on next page)

Notably, the 2023–2024 outbreak-causing strains formed two divergent clades: the Brazil and western Amazon basin (Peru, Colombia, and Ecuador) clades (Fig. 2A–C and Supplementary Fig. S1–S3). Specifically, the 2023–2024 strains identified in Brazil (containing the sequence sampled from French Guiana in 2020 (Gaillet et al., 2021)) are descendants of a monophyletic clade that includes the ILMD_TF29 strain, isolated from a reported case in Brazil in 2015 (Naveca et al., 2018). In parallel, the 2023–2024 strains identified in northern Peru and southern Colombia (Usuga et al., 2024) belong to the monophyletic clade together with the sequences sampled from 2016 to 2022 in Peru, Colombia, and Ecuador. Nonetheless, three out of seven 2023–2024 Peru strains (FPM01282, FPM01278, and FPM01287, isolated from southern Peru) are highly identical to the 2023–2024 Brazil sequences (e.g., LACENPR_ILMD_9982IOM, LVM_ILMD_ZDC-594, LACENAC_ILMD_7055) (Fig. 2A–C).

Collectively, these findings underscore the substantial genetic evolution of OROV over time and suggest that the current outbreak in Latin America is driven by the spread of locally circulating strains and cross-border importation further exacerbates the outbreak.

Increasing tendency in OROV substitution rates from 1955 to 2024

The high rate of mutagenesis in OROV genome is one of the key factors contributing to genetic diversity. Next, we estimated the genetic substitution rates of the L, M and S segments using the root-to-tip regression method (Fig. 2D–F) (Drummond et al., 2003). Dramatic temporal signals were observed in the L (Fig. 2D), M (Fig. 2E) and S (Fig. 2F) segment datasets. Substitution rates were then inferred for each segment from 1955–2024 (Fig. 2G). The global substitution rates were broadly consistent across segments: the L segment exhibited the highest rate (8.39E−4 substitutions/site/year, s/s/y), followed by the S segment (7.20E−4 s/s/y), and the M segment (6.90E−4 s/s/y). Notably, the substitution rates of both L, M segments have shown tendency towards higher rates over time (Fig. 2G). For instance, the substitution rate of the L segment increased from 2.08E−4 (1955–1989) to 1.16E−3 (1990–2024) s/s/y, and the M segment from 2.08E−4 (1955–1989) to 9.89E−4 (2020–2024) s/s/y (Fig. 2G). Consistently, these findings were further corroborated by a time-heterogeneous epoch model, which consistently revealed higher substitution rates for the 1990–2024 period compared to 1955–1989 across all three segments (Supplementary Fig. S4) (Sagulenko et al., 2018; Kocher et al., 2021). In conclusion, these results suggest that the substitution rate of OROV has exhibited an increasing tendency in recent decades relative to the earlier epoch.

Impact of genetic substitutions on amino acid and structural changes of viral proteins across evolutionary lineages

To investigate the impact of the high genetic substitution rate on amino acid changes, the amino acid consequences of OROV-encoded proteins were mapped (Fig. 3A, G, and H). Overall, 2.4% (54/2252) amino acids of the L segment encoding RdRp and 1.8% (26/1420) amino acids of the M segment encoding glycoproteins accumulated mutations from 1955 to 2024 (Fig. 3A and H), whereas the proteins encoded by the S segment were highly conserved (Fig. 3G). Specifically, the amino acids of L and M-encoded proteins remain stable until 1999. However, approximately 50% of observed mutations were acquired between 2000 and 2019, with the remaining 50% emerging during the four-year period from 2020 to 2024 (Fig. 3A and H), coinciding with the observed increase in substitution rates over time (Fig. 2G, Supplementary Fig. S4).

To assess the functional implications of these mutations, we visualized their impact on 3D protein structures constructed using AlphaFold3 (Abramson et al., 2024). The analysis focused on RdRp (Fig. 3B–F) and the spike domain of Gc glycoprotein (Fig. 3I–M), and revealed structural changes with potential functional consequences across multiple domains.

For RdRp, mutations were dispersed across several functional regions, including the Core lobe domain, palm domain, Cap-binding domain, and Zinc binding domain (Fig. 3A). For instance, the V1693I mutation was located within the RNA-protein contact active site cavity (Arragain et al., 2020) (Fig. 3F). Epidemic strains from the 2023–2024 outbreaks in Brazil and the western Amazon basin shared some mutations but also exhibited differences in specific positions (Fig. 3D and E). The Gc glycoprotein's head domain, along with Stem domains I and II, forms the trimeric spikes on the OROV envelope (Fig. 3I), critical for virion invasion and the primary target of the neutralizing antibody response (Hellert et al., 2019). Notably, mutations in the spike domain are predicted to alter its spatial conformation. Strains from Brazil accumulated 8 mutations in the spike domain (Fig. 3L), whereas those from the western Amazon basin acquired 35 mutations (Fig. 3M). Collectively, these findings suggest that divergent OROV lineages in Brazil and the western Amazon basin may have been subject to different selective pressures, contributing to distinct evolutionary trajectories.

OROV strains isolated from the 2023–2024 outbreak are universally reassortants

The tri-segmented genome of OROV bestowed the capacity for both reassortment (Naveca et al., 2024; Scachetti et al., 2024) and recombination. Reassortment is a process by which segmented genomes swap segments during co-infection of different viral strains within a single cell, whereas recombination is a process in which similar regions of their genomes pair together and exchange sequences. Both events can confer fitness advantages (or disadvantages) and drive genetic divergence. Correspondingly, the discordant tree topologies among the L, M, and S segments suggest the occurrence of reassortment events of OROV (Fig. 2A–C, Supplementary Fig. S1–S3) (Vasconcelos et al., 2011; Naveca et al., 2024; Scachetti et al., 2024). Therefore, we divided L segment into L_I and L_{II}, M segment into M_I, M_{II}, M_{III}, and S segment into $S_{I–V}$ clusters to scan reassortment events (Fig. 4A, and Supplementary Fig. S1–S3). Strikingly, compared to the first OROV strain identified in 1955 (TRVL9760, L_I, M_I, S_I), all OROV strains from the 2023–2024 outbreak were identified as reassortants (Fig. 4A).

To enhance the reliability of reassortment event identification, we concatenated the three segments (S, M, and L, datasets A, B, and C) for isolates with complete genomes and analyzed the concatenated alignment using seven independent methods implemented in RDP4 (Martin et al., 2015). Reassortment events were considered valid if supported by

Fig. 3. Structural analysis of OROV RdRp and Gc spike proteins. **A** The amino acid substitution dynamic of RdRp were analyzed and illustrated throughout the timeline from 1955 to 2024. The frequency of amino acid at each position was aligned and calculated based on the background set (1955–1989). The positions for which the most common character in the query set differs from that in the background set (1955–1989) were selected. The RdRp domains were labeled based on the RdRp of La Crosse virus (PDB 6Z6B) (Arragain et al., 2020). **B–E** The protein structure of RdRp of different time intervals was constructed by using AlphaFold3 (Abramson et al., 2024). The functional domains were labeled with colors the same as (**A**). The mutations were labeled with the color red. For RdRp, the mutations were dispersed on multiple functional domains, including the Core lobe domain, the Palm domain, the Cap-binding domain, and the Zinc binding domain. **F** Schematic representation of one mutation (V1693I) located in the RNA–protein contacts active site cavity. **G** same as (**A**) for S-encoding proteins. **H** same as (**A**) for M-encoding proteins. **I** The prominent trimeric spikes of the OROV envelope were constructed with AlphaFold3. The spike was composed of the head domain, stem domain I, and II of Gc protein (Hellert et al., 2019). **J–M** The mutations that occurred in the head domain, stem domain I, and II of Gc protein were labeled with the color red.

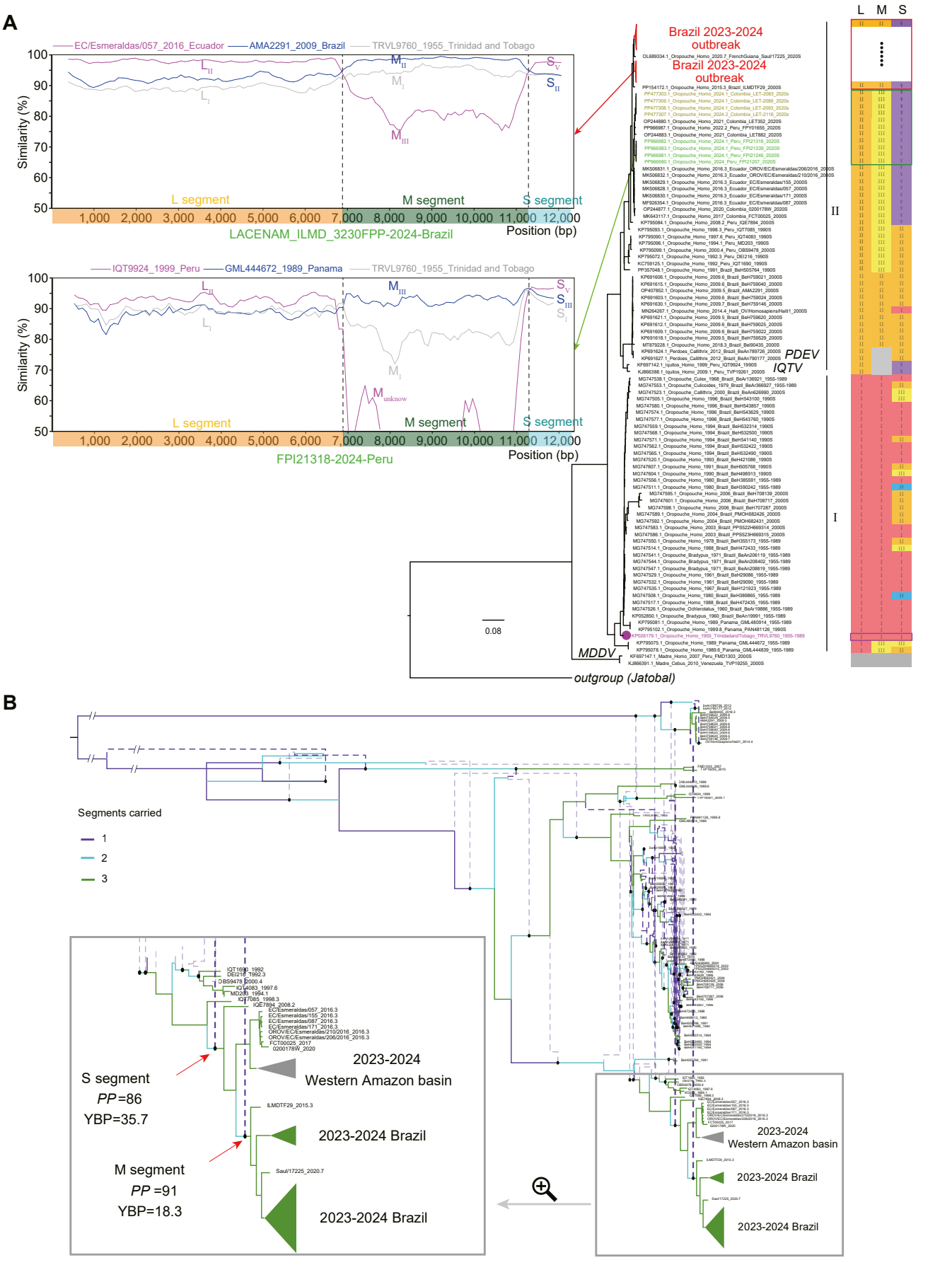

(caption on next page)

at least four of the seven detection methods available in RDP4 (Gutierrez et al., 2020). The analysis successfully identified the two previously known reassortants: IQTV (Aguilar et al., 2011) and PDEV (Tilston-Lunel et al., 2015) (Supplementary Table S4). Correspondingly, all strains isolated during the 2023–2024 outbreak were identified as reassortants (Supplementary Table S4).

These reassortment events were further verified using the Coalescent with Reassortment Constant Population (CoalRe) model (Fig. 4B) (Barido-Sottani et al., 2018; Muller et al., 2020). The CoalRe model estimated a reassortment rate of 0.036 (95% HPD: 0.027–0.042) per year per lineage. The M and S segment reassortment events that originated from the 2023–2024 outbreak were highly supported (*PP* = 91 and 86, respectively) and probably occurred around 2008 and 1989, respectively (Fig. 4B).

The timeline of successive reassortment events from 1955 to 2024 is illustrated in Fig. 5A and Fig. 5B, revealing the formation of two divergent lineages. For instance, the Brazil lineage, represented by strain LACENAM_ILMD_3230FPP, consists of L_{II}, M_{II}, S_V, whereas the western Amazon basin lineage, represented by strain IFPI21318, consists of L_{II}, M_{III}, S_V (Fig. 4A). Notably, all S segments of OROV identified after 2020 belong to the V cluster (Fig. 4A). Phylogenetic analysis indicated that cluster V first appeared in the Iquitos virus (IQTV) from Iquitos, a city located in northern Peru (Figs. 4A and 5B). The IQTV was a reassortant containing the S and L segments of OROV and the unknown M segment of a novel Simbu serogroup virus (Aguilar et al., 2011).

In addition, we scanned recombinant events by using seven independent methods implemented in RDP4 (Martin et al., 2015). Recombination was considered with evidence from at least four of the seven methods (Gutierrez et al., 2020). Intriguingly, we only identified 7/524 M, 1/524 L, and 0/524 S segments as potential recombinant sequences (Supplementary Table S5), indicating that recombination is rare and likely not a major driving force in OROV evolution.

Molecular clock analysis reveals an ancient origin of OROV, but a recent radiation out of South America

We analyzed all available S segment sequences (Fig. 1, dataset D, Supplementary Table S6) to construct the spatiotemporal evolutionary landscape of OROV. Our analysis revealed a negative correlation between OROV's nucleotide substitution rates and the timeline (Fig. 2G). Based on that, a time-dependent rate (TDR) model, dividing sequences into four epochs (1955–1989, 1990–2000, 2001–2019, and 2020–2024), was applied to estimate the time to the most recent common ancestor (tMRCA). We obtained an estimate indicating a strong TDR effect in dataset D (S segment, $\beta 1 = -0.539$, 95% HPD: −0.662 to −0.422). Estimated mean substitution rates for root, 1990–1999, 2000–2019, and 2020–2024 epochs were 2.49E−4, 3.40E−4, 5.02E−4, and 1.43E−3 s/s/y, respectively (Supplementary Fig. S5A). In comparison, the uncorrelated relaxed clock (UCLD) model produced an overall substitution rate of 1.49E−3 s/s/y, equivalent to the rate estimated for the 2020–2024 epoch by the TDR model (Supplementary Fig. S5A). This suggests that the UCLD model overestimates substitution rates and correspondingly underestimates divergence times (Supplementary Fig. S5B).

Accordingly, we retained the TDR-based estimates for downstream analyses. The median tMRCA of OROV S segment dataset D was estimated to date back to the 1740s [~284.7 years before present (YBP), 95% HPD: 217.6–359.1 YBP] (Fig. 6A, Supplementary Fig. S5B). Subsequently, S segment diversified into five clusters between the 1880s and 1970s (Fig. 6A). Specifically, cluster S_I was the oldest (tMRCA: ~128.8 YBP, 95% HPD: 106.5–258.2 YBP), whereas cluster S_{IV} (tMRCA: ~53.1 YBP, 95% HPD: 46.6–62.8 YBP) relatively younger. The cluster S_V formed in the 1900s (~110.9 YBP, 95% HPD: 78.2–148.1 YBP), was the only cluster associated with the 2023–2024 outbreak (Fig. 6A). Notably, the tMRCA estimated in this study predate previous findings, which suggested a median tMRCA of 1940 (95% HPD: 1916–1955) (Gutierrez et al., 2020). This discrepancy, attributed to the time-dependent rate phenomenon in viral evolution, provides new insights into OROV's origins.

Next, we employed a Bayesian discrete phylogeographic approach to investigate the areas of origin and propagation routes of OROV, and the Bayesian stochastic search variable selection (BSSVS) procedure was used to provide a sufficient description of viral dissemination. Bayesian phylogenetic analysis identified Brazil as the most probable ancestral location of OROV (Fig. 6A, root state posterior probability = 0.69). Between the 1800s and 1950s, OROV gradually spread to the Peru and Caribbean regions and was first discovered in Trinidad and Tobago in 1955 (Fig. 6B). From the 1970s to the 1990s, OROV spread to Panama, Colombia, Ecuador, and Haiti. From the 1990s to the 2010s, the virus became sporadic in multiple countries/regions and formed a bidirectional transmission route between Peru and Brazil. From 2020 to 2024, the number of infected individuals continuously increase, which eventually led to the large 2023–2024 outbreak and the virus further spread to new regions such as French Guiana. Two imported OROV cases recently identified in Italy (IRCCS-SCDC_1/2024 and IRCCS-SCDC_1442/2024) originated from Brazil, then spread to Cuba, and were further imported to Italy (Fig. 6B and C).

To evaluate the robustness of the model and dataset, Bayesian phylogenetic analyses were conducted using datasets A, B, and C (Supplementary Fig. S6). Results from datasets B and C were consistent, confirming similar evolutionary patterns. However, the L segment (dataset A) analysis suggested Peru as the ancestral location. Both the L segment (dataset A) (Supplementary Fig. S6B) and the M segment (dataset B) (Supplementary Fig. S6C) showed earlier tMRCA (~389.4 YBP, 95% HPD: 330.9–450.6 YBP; and ~2878.1 YBP, 95% HPD: 2163.7–3662.3 YBP, respectively) than those estimated based on the S segment dataset C (~225.8 YBP, 95% HPD: 140.2–283.6 YBP) (Supplementary Fig. S6A) and dataset D (~284.7 YBP, 95% HPD: 217.6–359.1 YBP) (Fig. 6A). These results suggest that the three segments may originate from different ancestors or have undergone unknown recombination events.

DISCUSSION

In this study, our in-depth phylogenomic analysis reveals that mutagenesis and reassortment cooperatively drive the accelerated evolution of OROV. This is similar to influenza A viruses, which are also single-stranded negative-sense RNA viruses with a segmented genome. For Influenza A, pandemics have been sparked by the emergence of reassortant strains with critical mutations that gain adaptation to human hosts (Taylor et al., 2023). Although the mutation-prone feature of OROV appears to be obvious (Gutierrez et al., 2020), the impact of reassortment and mutagenesis on its evolution remains largely underestimated. In fact, the wide range of reservoirs, including pale-throated sloths and non-human primates (Wesselmann et al., 2024), as well as the arthropod transmission route of OROV provide

Fig. 4. Phylogenetic and reassortment analysis of OROV. **A** Maximum-likelihood phylogenetic analysis of the L segment. For each isolate, the clusters (I to V) of L, M, and S were annotated based on phylogenetic analysis (Vasconcelos et al., 2011). The left panel illustrated the nucleic acid similarity plot of two representative 2024 outbreak-causing strains from Brazil (LACENAM_ILMD_3230FPP) and Peru (FPI21318), respectively. **B** Reassortment network of OROV complete genomes. Reassortment network of OROV complete genomes was estimated using CoalRe and visualized via icytree.org (https://icytree.org/). Reassortment events are indicated by dashed lines. The color of each branch represents the number of segments carried by that branch. The intensity of the dashed line color indicates the posterior probability (*PP*) value: darker shades denote $PP > 70$, while lighter shades denote $PP < 70$. For reassortment events associated with the 2024 OROV outbreak, their respective *PP* values, segment names, and Years Before Present (YBP) are labeled on the corresponding nodes.

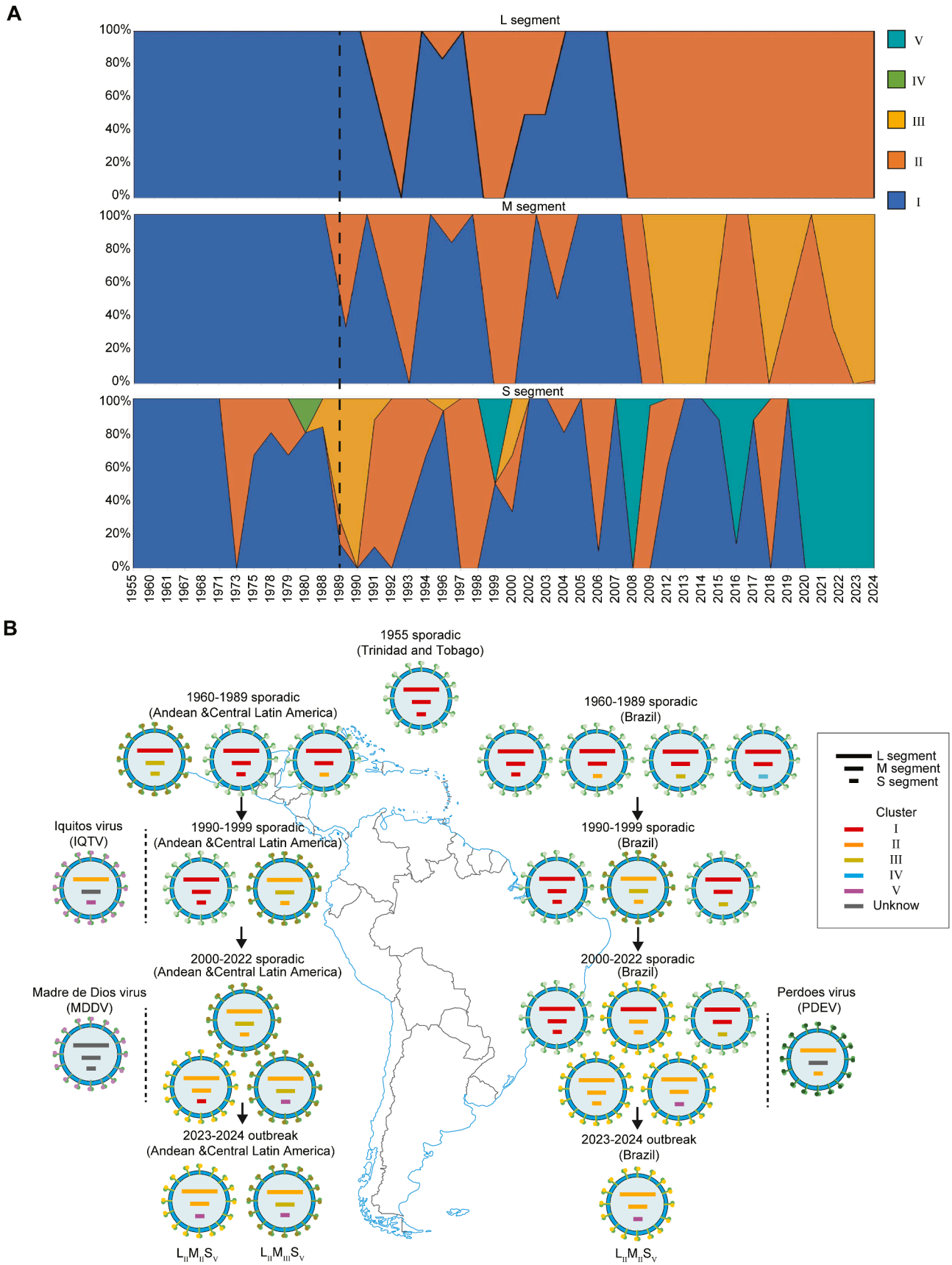

Fig. 5. The timeline of successive reassortment events from 1955 to 2024. **A** The composition ratio of subclusters (L, M, and S segments) varies over time. Years without sequences have been deleted. The dashed line distinguishes two time periods (1955–1989, 1990–2024). **B** Schematic representation of the reassortment dynamics of two divergent 2023–2024 outbreak lineages throughout the timeline (1955–2024). The reassortment dynamics of OROV in each period were illustrated based on the phylogenetic and reassortment network analyses of L, M, and S segments (Supplementary Fig. S1–S3; Table S4, and Fig. 4B).

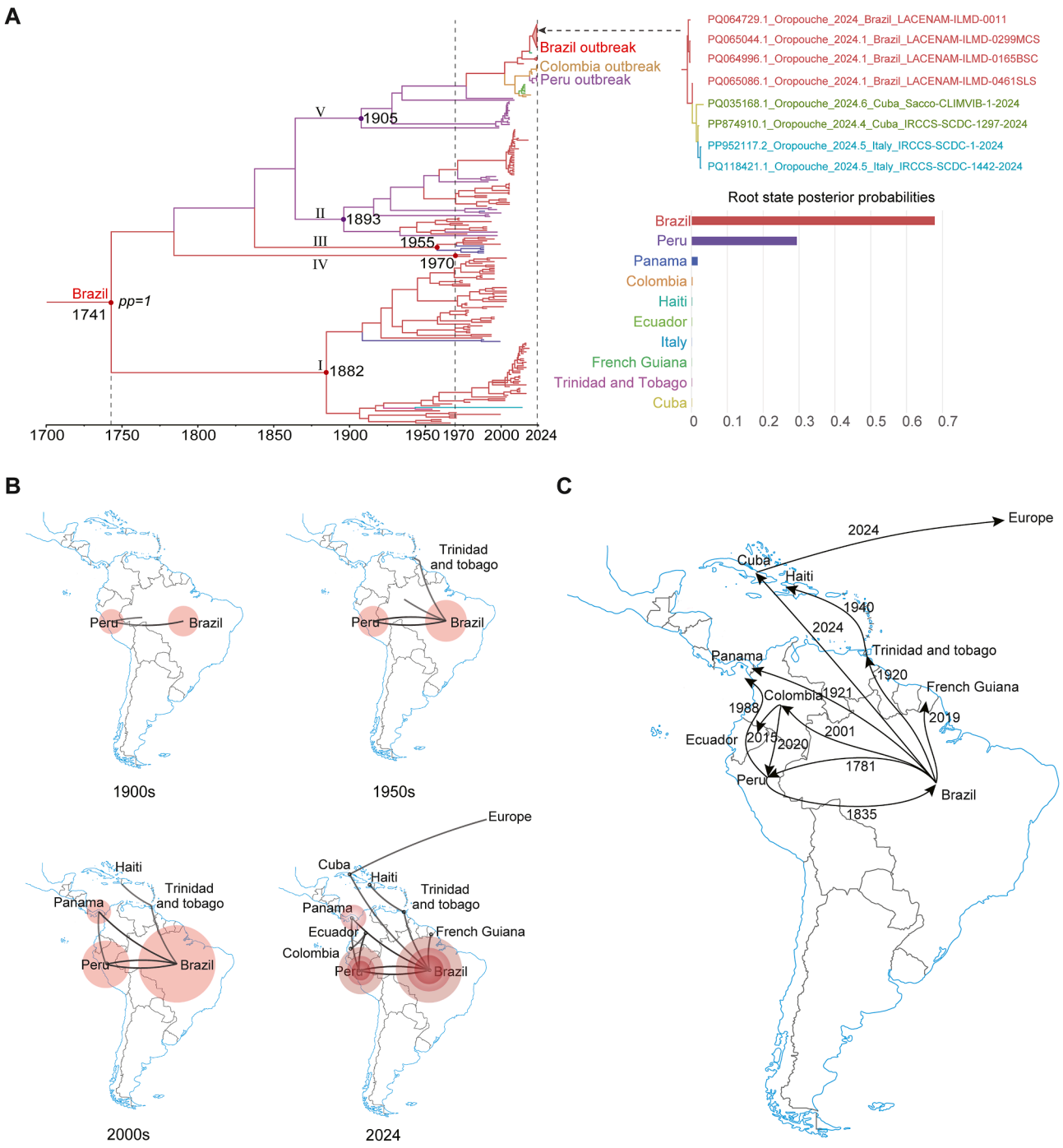

Fig. 6. Time-scaled phylogenetic analyses of OROV and its propagation roadmap. **A** The Maximum Clade Credibility (MCC) tree with a time-dependent rate of OROV was generated based on the S segment dataset D. The geographic regions were labeled with the indicated colors. The root state posterior probabilities were calculated using TreeAnnotator. **B** The transmission roadmap of OROV from the 1740s to 2024 was illustrated by spreaD3 based on the MCC tree (S segment dataset D). The sizes of red circular indicate the relative intensity of local spread, with larger circles indicating a higher number of tree branches at that location through time (He et al., 2022). **C** The transmission roadmap of OROV was summarized on the map.

ample opportunities for both reassortment and mutagenesis (Briese et al., 2013; Elliott, 2014). We demonstrate the changes in virus amino acid sites and structural predictions from 1955 to the present (Fig. 3). Interestingly, accumulated mutations are associated with structural changes in viral proteins. For example, the head domain, stem domain I, and II of Gc protein form trimeric spikes of the OROV envelope (Fig. 3H–M), which are essential for entering host cells and are the major target of neutralizing antibodies (Hellert et al., 2019). Some of the mutations (T857A in the L segment, and R1342K in the M segment) have been specifically associated with fatal cases (Iani et al., 2024). Unfortunately, we are unable to access the viral sequences from cases with severe complications, including cases of vertical transmission and fatalities (Martins-Filho et al., 2024). Profiling the mutation landscapes and reassortment events in these strains would be crucial to understanding their potential roles in pathogenesis. Eventually, functional investigations, such as using reverse genetics (Acrani et al., 2015) and robust experimental models (Gunter et al., 2024), are required to demonstrate the causative relation.

Reassortment and genetic drift are important molecular genetic mechanisms that confer the genetic diversity in segmented RNA viruses in nature (Simon-Loriere and Holmes, 2011). Mechanistically, reassortment can produce abrupt, large-scale shifts in viral phenotype by exchanging intact genome segments and thereby combining distinct functional modules responsible for replication and entry (Mcdonald et al., 2016). For 2024 outbreak strains, CoalRe and whole-genome phylogenetic analysis implicate M-segment reassortment in the origin of two geographically distinct lineages: one in Brazil (L_{II}, M_{II}, S_V) and another in the western Amazon basin (encompassing Peru, Colombia, and Ecuador, L_{II}, M_{III}, S_V) (Fig. 2A–C, Fig. 4). Specifically, compared to the strains isolated between 1955 and 1989, the Brazil lineage accumulated eight mutations in the spike domain (Fig. 3L), whereas the western Amazon basin lineage acquired 35 mutations (Fig. 3M). Such reassortment-driven genomic reshuffling, together with lineage-specific amino-acid changes, is therefore expected to have functional consequences for virus entry, antigenicity and host tropism. For instance, the K614 and F620 mutations found in the Brazil and western Amazon basin lineages are located at the apex of the spike head domain and may modulate receptor-binding affinity (Supplementary Fig. S7B) (Hellert et al., 2019). In addition, the S578 and N683 substitutions in the western Amazon lineage lie at the protomer–protomer interface within the trimeric head domain, where they may perturb inter-subunit contacts and remodel the antigenic surface of the spike (Supplementary Fig. S7C). The localized circulation of these lineages further supports those differential selective pressures have driven their divergence. Functional relevance is supported by a recent report showing increased replication efficiency for a Brazil-lineage isolate (AM0088) relative to a historical prototype (BeAn19991,1960s) (Scachetti et al., 2024). However, differences in replication capability and propagation efficiency between the Brazil and western Amazon basin lineages remain unclear. It is crucial to assess their replication efficiency in mammalian cells and transmission efficiency via insect vectors (Mcgregor et al., 2021; Scachetti et al., 2024). Moreover, our phylogenetic analysis (Fig. 2A–C), in conjunction with previous epidemiological data (Moreira et al., 2024; Usuga et al., 2024), suggests that cross-border transmission has facilitated the co-circulation of the Brazil and western Amazon basin lineages within the Amazon basin. This co-circulation raises concerns about the potential emergence of new reassortant strains. Although the structural predictions are computational but generate clear, testable hypotheses that link reassortment and specific amino-acid changes to potential shifts in viral fitness and outbreak potential.

Nucleotide substitution rates in viruses are generally inversely correlated with the measurement timescales (Ho et al., 2005; Aiewsakun and Katzourakis, 2016). For OROV, accelerated substitution rates have been observed from 1955 to 2024 (Fig. 2G). To better understand OROV's evolutionary history, we divided the timeline into four epochs (1955–1989, 1990–2000, 2001–2019, and 2020–2024) and constructed time-scaled maximum clade credibility (MCC) trees for the L, M, and S segments. Consistent with previous research (Gutierrez et al., 2020), the tMRCA of the L segment and M segment predate that of the S segment (Supplementary Fig. S6). Additionally, applying a time-dependent rate model further amplified the tMRCA gap among the three segments (Gutierrez et al., 2020). Phylogeographic analysis revealed propagation routes inferred from L segment sequences that differ from the origin regions suggested by the S and M segments. This significant disparity in tMRCA estimates and origin regions suggests that the three segments may have originated from different ancestral lineages or undergone unrecognized recombination events (Saeed et al., 2001; Aguilar et al., 2011; Briese et al., 2013; Ladner et al., 2014; Tilston-Lunel et al., 2015; Gutierrez et al., 2020). Our findings underscore the importance for comprehensive, long-term whole-genome surveillance, encompassing all three segments (L, M, and S), to fully describe the transmission and reassortment dynamics of OROV. However, similar to other RNA viruses, the OROV RNA genome degrades rapidly in the environment, making it impossible to obtain ancient genomes to calibrate the temporal signals over a long-time scale. Thus, owing to the TDR phenomenon (Ho et al., 2005), these insurmountable restrictive factors may lead to underestimation of tMRCA to some extent (Membrebe et al., 2019). Additionally, the scarcity of available OROV sequences prior to the 2023–2024 outbreak introduces potential sampling biases that could influence evolutionary analyses. In particular, the underrepresentation of sequence diversity in earlier decades may result in an underestimation of long-term substitution rates, potentially exaggerating the apparent acceleration observed in recent years. Despite these challenges, our study utilized all publicly available OROV full-length genome sequences and applied a time-dependent rates model, providing insights into the evolutionary history of OROV. To the best of our knowledge, this approach represents the most reliable method currently feasible based on the available OROV genomic resources.

CONCLUSIONS

Currently, there is major emphasis on identifying the possible factors that drive the current outbreak, including viral adaption, climate change, human and animal mobility, and deforestation (Graf et al., 2024; Iani et al., 2024; Naveca et al., 2024; Scachetti et al., 2024; Wesselmann et al., 2024). However, our findings highlight that comprehending the genomic evolution is equally important for understanding the emergence of the OROV outbreak. Additionally, further in-depth functional investigations are urgently required to effectively respond to this ongoing outbreak and prepare for future ones.

MATERIALS AND METHODS

Establishment of datasets

All available *Orthobunyavirus oropoucheense* sequences (2147 sequences, accessed on October 10th, 2024) were collected from the GenBank (https://www.ncbi.nlm.nih.gov/genbank). “Oropoucheense” [All Fields] OR “Oropouche” [All Fields] was used as the search term. Sequence-related information, e.g., accession ID, strain ID, segment, collection date, geographical location name, host, length, and country was also retrieved by using PhyloSuite (v1.2.2) (Zhang et al., 2020). Sequences were divided into L, M, and S segments based on the information provided by NCBI. Only the strains with the all three segments were included. In total, 524 strains containing all three segments were included in the dataset A–C (Fig. 1, Supplementary Table S1–S3). Correspondingly, the amino acid sequences of all coding regions of each strain in dataset were downloaded from the NCBI protein database (https://www.ncbi.nlm.nih.gov/protein). To investigate changes in substitution rates, strains were divided into two 34-year groups: 1955–1989 and 1990–2024.

In order to reveal the spread and origin of OROV, we constructed the dataset D of S segment which included all available S segment sequences to preserve more comprehensive “geographic” and “collected data” information (Supplementary Table S6). The Madre de Dios virus was excluded due to the poor homology of its three segments to OROV.

For further details regarding the datasets constructed and used, please refer to Supplementary Table S1–S3, and Table S6.

Phylogenies and Bayesian analysis

Sequences were aligned using the MAFFT 7 (Katoh and Standley, 2013). IQ-TREE (version 2.2.0) (Minh et al., 2020) and FastTree (Price et al., 2009) were used to construct the maximum likelihood (ML) phylogenetic tree (performing 1000 replicates of bootstrap). The Jatobal virus (strain ID: BeAn 423,380) was used as the out-group. ModelFinder (in IQ-TREE package) was employed to identify the best model for the ML phylogenies and Bayesian analysis. Clockor2 was used to check the temporal signal (Featherstone et al., 2024). The distinct cluster was

identified considering the bootstrap support of more than 75% and the branch length (>0.001) (Cui et al., 2014).

To estimate the temporal and spatial dynamics of OROV on various continents, we constructed time-scaled phylogenetic trees using BEAST v1.10.4 and BEAGLE (Suchard et al., 2018). Markov chain Monte Carlo (MCMC) runs 250 million generations under a Bayesian Skyline demographic model (Suchard et al., 2018). A time-dependent-rate model and an uncorrelated lognormal relaxed clock (UCLD) model were used as previously described (Ding et al., 2024). Specifically, we divided the timeline to 4 epochs (1955–1989, 1990–2000, 2001–2019, and 2020–2024). We used normal priors with mean = −5.09 (β0) and 0 (β1) and standard deviation = 5 and 5 for the intercept and slope coefficients of the log-linear relationship between the substitution rate and time, respectively (corresponding to an expected rate of ~6E−3 substitution/site/year at time 0 and no prior assumption on the direction of the relationship). The Bayesian MCMC output was analyzed using Tracer (version 1.7). The first 10%–30% of the states from each run were discarded as burn-in. Trees were summarized as maximum clade credibility (MCC) trees using TreeAnnotator (in the BEAST package) and then visualized in FigTree (version 1.4.4). We employed a Bayesian discrete phylogeographic approach to investigate the areas of origin and propagation routes of OROV, and the Bayesian stochastic search variable selection (BSSVS) procedure was used to provide a sufficient description of viral dissemination (Lemey et al., 2009). Discrete geographic areas were defined based on the geographical regions of the countries from which the sequences were sampled. SpreaD3 was used to visualize the MCC trees (Bielejec et al., 2016).

Recombination and reassortment analyses

Recombination refers to intra-segmental sequence rearrangement, involving the joining of genetic material from different viral lineages within a single genomic segment. The S, M and L segment sequences of 524 strains were scanned for recombinant, respectively, using the seven methods (RDP GENECONV, Bootscan, Maxchi, Chimaera, SiSscan, 3Seq) implemented in RDP4. Sequences were identified as recombination with the support of at least four methods simultaneously (Gutierrez et al., 2020). $P < 0.05$ is considered statistically significant.

Reassortment refers to inter-segmental genomic shuffling, where entire genome segments (L, M, or S) are exchanged between co-infecting viruses, and generating progeny with novel segment combinations. The phylogenetic trees of three segments were used to identify the reassortment events. The strains are labeled as the reassortant if their three segments are not in the same cluster in the ML and MCC trees (Tilston-Lunel et al., 2015; Naveca et al., 2024). And then, the three segments were concatenated and scanned for reassortment using the seven methods (RDP GENECONV, Bootscan, Maxchi, Chimaera, SiSscan, 3Seq) implemented in RDP4 (Martin et al., 2015). Sequences were identified as reassortment with the support of at least four methods simultaneously (Gutierrez et al., 2020). $P < 0.05$ is considered statistically significant. Furthermore, OROV reassortment events were also reconstructed using the Coalescent with Reassortment Constant Population (CoalRe) model as implemented in the BEAST2 package and following previous studies (Barido-Sottani et al., 2018; Muller et al., 2020; Naveca et al., 2024). The reassortment rate parameter was assigned an exponential prior with a mean of 0.25, consistent with previous studies (Muller et al., 2020; Naveca et al., 2024).

Identify the amino acid mutations

Amino acid sequences of all coding regions of each strain were downloaded from the NCBI protein database (https://www.ncbi.nlm.nih.gov/protein). The frequency of each amino acid at each position in an alignment for the query set and background set (1955–1989) was calculated by VESPA (Korber and Myers, 1992) and selected the positions for which the most common character in the query set differs from that in the background set (1955–1989).

Structural analysis of OROV proteins

Three-dimensional structural models of the OROV RdRp (L segment) and Gc glycoprotein spike domain (M segment) were generated using the AlphaFold3 web interface (https://alphafoldserver.com/) (Abramson et al., 2024). The modeling was performed in 'single sequence' (monomer) mode for the full-length RdRp, and in 'three sequences' (trimer) mode for the spike domain. No custom template restrictions or advanced MSA parameters were modified. The server's built-in pipeline automatically performed MSA generation, template search (Use PDB templates with cutoff November 10, 2024). For each structure, five models were generated with three recycles, and were ranked by the predicted template modeling (pTM) and interface predicted template modeling (ipTM) score. The top-ranked model with the highest pTM and ipTM score was selected for downstream visualization and mapping of lineage-specific amino acid substitutions. The pTM score above 0.5 and the ipTM score above 0.8 represent confident high-quality predictions. The annotation of functional domains in RdRP region is based on the previously reported La Crosse virus (*Orthobunyavirus*) (Arragain et al., 2020).

DATA AVAILABILITY

All sequences were collected from NCBI and listed in Supplementary Table S1–S3, and Table S6.

ETHICS STATEMENT

This article does not contain any studies with human or animal subjects performed by any of the authors.

AUTHOR CONTRIBUTIONS

Yibo Ding: Conceptualization, data curation, funding acquisition, methodology, software, visualization, writing-original draft, writing-review & editing. Jiajing Li: Data curation, formal analysis, investigation, writing-review & editing. Xin Wang: Data curation, formal analysis, investigation, writing-review & editing. Simone Malagò: Writing-review & editing. Amaro Nunes Duarte-Neto: Writing-review & editing. Xiaohui Ding: Writing-review & editing. Fang Qin: Writing-review & editing. Michela Deiana: Writing-review & editing. Concetta Castilletti: Writing-review & editing. Hongbo Guo: Conceptualization, data curation, funding acquisition, writing-original draft, writing-review & editing. Qiuwei Pan: Conceptualization, data curation, formal analysis, writing-original draft, writing-review & editing. Wenshi Wang: Conceptualization (lead), data curation, formal analysis, funding acquisition, writing-original draft, writing-review & editing.

CONFLICT OF INTEREST

The authors declare that they have no conflict of interest.

ACKNOWLEDGMENTS

This work is supported by the National Natural Science Foundation of China, 32270161, 82302506. Research Grant of Jiangsu Commission of Health, ZD2021036. The Starting Grant for Talents of Xuzhou Medical University, D2021007, D2021008, D2024017. The Natural Science Foundation of the Jiangsu Higher Education Institutions of China (23KJD310005, 23KJB310028, 24KJD310005).

We thanks all the researchers who have publicly shared their OROV sequences in GenBank, including Gabriel da Luz Wallau, Naveca, F.G., Almeida, T.A.P., Souza, V., Nascimento, V., Silva, D., Nascimento, F., Mejía, M., Oliveira, Y.S., Rocha, L., Xavier, N., Lopes, J., Maito, R., Meneses, C., Amorim, T., Fé, L., Camelo, F.S., Silva, S.C.A., Melo, A.X., Fernandes, L.G., Oliveira, M.A.A., Arcanjo, A.R., Araújo, G., André, Júnior, W., Carvalho, R.L.C., Rodrigues, R., Albuquerque, S., Mattos, C., Silva, C., Linhares, A., Rodrigues, T., Mariscal, F., Morais, M.A., Presibella, M.M., Marques, N.F.Q., Paiva, A., Ribeiro, K., Vieira, D., Queiroz, J.A.D.S., Passos-Silva, A.M., Abdalla, L., Santos, J.H., Figueiredo, R.M.P., Cruz, A.C.R., Casseb, L.N., Chiang, J.O., Frutuoso, L.V., Rossi, A., Freitas, L., Campos, T.L., Wallau, G.L., Moreira, E., Lins, Neto, R.D., Alexander, L.W., Sun, Y., Filippis, A.M.B., Gräf, T., Arantes, I., Bento, A.I., Delatorre, E., Bello, G., Mejia, M., Oliveira, Y., Naveca, F., Sacchi, C.T., Campos, K.R., Goulart, J.P., B, eira, A.C., MotaPereira, F., Leal, A., Santos, S.P.O., Barbosa, A.C.F.N.S., SaoPedro, M., RibeirodeSouza, D., Guimaraes, N., Fonseca, V., Giovanetti, M., JuniorAlcantara, L.C., Lessa, A.A., CostaSaavedra, R., Tome, L.M.R., Iani, F.C.M., Barros, R.M., Purificacao, S.M.O., PradodeJesus, J., RosarioFonseca, R., ValencaAraujo, M.L., Graf, T., Ferreira, C.N., Pizzato, B.R., Goncalves, S., Araujo, S.I.R., Belettini, S.A.A., Rovaris, D.B., Machado, M.H., Zanluca, C., DuartedosSantos, C., Dutra, J.V.R., Reis, C.R., Moreira, F.R.R., Aguiar, R.S., Carvalho, A.H.B., Rios, J.S.H., Ribeiro, M.O., Arruda, M.B., Alvarez, P., Souza, R.P., Voloch, C., Zauli, D.A.G., Gatti, F.D., Mendonca, G.C., Nodari, J.Z., Sousa, T.J., Rodrigues, R.R., Almeida, T., Casseb, L., Chiang, J., Cruz, A.C., Rodrigues, J.T., Araujo, G., Barros, D., Wallau, G., Vasconcelos, H.B., Nunes, M.R., Casseb, L.M., Carvalho, V.L., PintodaSilva, E.V., Silva, M., Casseb, S.M., Vasconcelos, P.F., Nunes, M.R.T., Rodrigues, S.G., Araujo, G.C.B., TravassosdaRosa, A.P.A., Vasconcelos, P.F.C., Azevedo, R.S., Bensabath, G., Pinto, A.Y., Martins, L.C., Monteiro, H.A., Saeed, M.F., Wang, H., Nunes, M., Weaver, S.C., Shope, R.E., Watts, D.M., Tesh, R.B., Barrett, A.D., Casseb, S.M.M., Silva, E.V.P., Silva, M.O., Casseb, L.M.N., deSouza, W.M., Savji, N., Figueiredo, M.L., Cardoso, J.F., daSilva, S.P., daSilvadeLima, C.P., IanLipkin, W., Palacios, G., TravassosdaRosa, J.F.S., Silva, S.P., Lima, C.P.S., Oliveira, L.F., Vasconcelos, J.M., DaSilva, D.E.A., Guzman, H., Vianez-Junior, J.L.S.G., Fonseca, L.M.S., Souza, R.R.M., B, era, A.A.C., Campos, G.S., Sardi, S.I., deSouzaCosta, M.C., SiqueiraMaia, L.M., CostadeSouza, V., Gonzaga, A.M., CorreadeAzevedo, V., RamosMartins, L., ChavezPavoni, J.H., GomesNaveca, F., DezengriniSlhessarenko, R., Carvalho, R.H., Cardoso, B.F., Serra, O.P., Heinen, L.B., Zuchi, N., Souza, V.C., Naveca, F.G., Santos, M.A., Slhessarenko, R.D., Dezengrini-Slhessarenko, R., BastosMde, S., Figueiredo, L.T., Monte, R.L., Lessa, N., PintodeFigueiredo, R.M., Gimaque, J.B., PivotoJoao, G., Ramasawmy, R., Mourao, M.P., RamirezPavon, J.A., Neves, N.A.S., deAzevedo, F.K., deFigueiredoJunior, J.A.B., Tauro, L.B., Jacob, L.C., Reis, M.G., Ribeiro, G.S., Mondini, A., Moraes, M.M., deOliveira, I.P.F., Orechovesky, S.A., Pereira, W.V.G.E., Gusmao, A.F., Valentini, S.R., Zanelli, C.F., Bronzoni, R.V.M., Schmidt, D.J., Milhim, B., Dutra, K.R., Pacca, C.C., DutraSilva, G.C., Terzian, A.C.B., Nogueira, M.L., Bernardes-Terzian, A.C., de-Moraes-Bronzoni, R.V., Drumond, B.P., DaSilva-Nunes, M., da-Silva, N.S., Urbano-Ferreira, M., Speranca, M.A., Acrani, G.O., Tilston-Lunel, N.L., Spiegel, M., Weidmann, M., Dilcher, M., radedaSilva, D.E., Elliott, R.M., White, S.K., Elbadry, M.A., Morris, J.G.Jr., Lednicky, J.A., AzevedoRdo, S., daRosa, A.P., Wise, E.L., Logue, C.H., Mellors, J., Atkinson, B., Marquez, S., Zapata, S., Paz, V., Trueba, G., Gutierrez, B., Pybus, O.G., Jackson, S.K., Fejer, G., Pullan, S.T., Mosquera, J.D., Mena, S., Ciuoderis, K.A., Berg, M.G., Perez, L.J., Hadji, A., Perez-Restrepo, L.S., Aristizabal, L.C., Forberg, K., Yamaguchi, J., Cardona, A., Weiss, S., Qiu, X., Hern, ez-Ortiz, J.P., Averhoff, F., Cloherty, G.A., Osorio, J.E., Ampuero, J.S., daSilva, V.G., daSilva, A.F., Machado, L.C., deLima, G.B., Silva, K.M.P., daCosta, M.M.O.M., Falcao, D.A., Vasconcelos, A.P., Azevedo, E.A.N., daSilva, C.C., Acioli-Santos, B., Paiva, M.H.S., deMorais, C.N.L., Justino, M.C.A., Matos, H.J., Cabeca, H.L.S., Henriques, D.F., , rade, G.S.S., Azevedo, R.S.S., Hughes, J., daSilva, D.E., Watanabe, A., Marano, J.M., Bowen, R.A., Bosco-Lauth, A.M., Espinoza, A., Castillo, R., deBruycker-Nogueira, F., BispodeFilippis, A.M., Aguilar, P.V., Russell, K., Suarez, L., Cespedes, M., Montgomery, J.M., Kochel, T.J., Guevara, C., Montgomery, J.M., , Halsey, E.S., Deiana, M., Malago', S., Piubelli, C., Castilletti, C., Mori, A., Matucci, A., Chesini, L., Pomari, E., VanDuffel, L., Cristini, F., Gobbi, F.G., Giacomelli, A., Vezzosi, L., Gori, A., Antinori, S., Cereda, D., Gismondo, M.R., Medeiros, D.B.A., Limonta, D., Peres-Restrepo, L.S., Ciouderis, K., Osorio, J.R., Nogueira, J.S., Maeda, A.Y., Moreira, H.M., Sgorlon, G.O., Queiroz, J.A.S., Roca, T.P., Ribeiro, J., Teixeira, K.S., Araujo, A.O., Gasparelo, N.W.F., Santos, A.O., Lugtenburg, C.A.B., Roque, R.A., Salcedo, J.M.V., Pereira, D.B., Vieira, D.S., Gaillet, M., Pichard, C., Restrepo, J., Lavergne, A., Perez, L., Enfissi, A., Abboud, P., Lambert, Y., Ma, L., Monot, M., Demar, M., Djossou, F., Servas, V., Nacher, M., rieu, A., Prudhomme, J., Michaud, C., Rousseau, C., Jeanne, I., Duchemin, J.B., Epelboin, L., Rousset, D., Lima, A.F.C., Ladner, J.T., Lofts, L., TravassosdaRosa, A., Wiley, M.R., Gestole, M.C., Rosen, G.E., JKochel, T., Lipkin, W.I., Barrett, A.D.T., deLima, C.P.S., Costa, M.C., Maia, L.M., Azevedo, V.C., Pavoni, J.H., Martins, L.R., Bastos, M.S., Oliveira, C.M., Chave, J.H., Terzian, A.C., Silva-Nunes, M., Silva, N.S., Ferreira, M.U., OlszanskiAcrani, G., Vascomcelos, P.F.C., Cuideras, K.A., Carajal-Aristizabal, L., Ochoa, M., Gomez, D., Cruz, C.D., Troncos, G.M., Silva, M.S., Troncos, G., Espejo, V., Mancon, A., Mileto, D., Gagliardi, G., Ciuoderis, K., Usuga, J., Moreno, I., Vargas, V., Arevalo-Arbelaez, A.J., Tirera, S., Wiley, M., and Lipkin, I.

APPENDIX A. SUPPLEMENTARY DATA

Supplementary data to this article can be found online at https://doi.org/10.1016/j.virs.2025.09.009.

REFERENCES

Abramson, J., Adler, J., Dunger, J., Evans, R., Green, T., Pritzel, A., Ronneberger, O., Willmore, L., Ballard, A.J., Bambrick, J., et al., 2024. Accurate structure prediction of biomolecular interactions with AlphaFold 3. Nature 630, 493–500.

Acrani, G.O., Tilston-Lunel, N.L., Spiegel, M., Weidmann, M., Dilcher, M., Andrade Da Silva, D.E., Nunes, M.R.T., Elliott, R.M., 2015. Establishment of a minigenome system for oropouche virus reveals the S genome segment to be significantly longer than reported previously. J. Gen. Virol. 96, 513–523.

Aguilar, P.V., Barrett, A.D., Saeed, M.F., Watts, D.M., Russell, K., Guevara, C., Ampuero, J.S., Suarez, L., Cespedes, M., Montgomery, J.M., Halsey, E.S., Kochel, T.J., 2011. Iquitos virus: a novel reassortant Orthobunyavirus associated with human illness in Peru. PLoS Neglected Trop. Dis. 5, e1315.

Aiewsakun, P., Katzourakis, A., 2016. Time-dependent rate phenomenon in viruses. J. Virol. 90, 7184–7195.

Anderer, S., 2024. Oropouche virus spreads to new regions in Latin America. JAMA 332, 954.

Anderson, C.R., Spence, L., Downs, W.G., Aitken, T.H., 1961. Oropouche virus: a new human disease agent from Trinidad, West Indies. Am. J. Trop. Med. Hyg. 10, 574–578.

Arragain, B., Effantin, G., Gerlach, P., Reguera, J., Schoehn, G., Cusack, S., Malet, H., 2020. Pre-initiation and elongation structures of full-length La Crosse virus polymerase reveal functionally important conformational changes. Nat. Commun. 11, 3590.

Baer, K., Arora, I., Kimbro, J., Haider, A., Mott, M., Marshall, K., Wu, H.M., Fairley, J., Piantadosi, A., Myers, D.R., Waggoner, J.J., 2024. Iquitos virus in traveler returning to the United States from Ecuador. Emerg. Infect. Dis. 30, 2447–2451.

Barido-Sottani, J., Boskova, V., Plessis, L.D., Kuhnert, D., Magnus, C., Mitov, V., Muller, N.F., Pecerska, J., Rasmussen, D.A., Zhang, C., Drummond, A.J., Heath, T.A., Pybus, O.G., Vaughan, T.G., Stadler, T., 2018. Taming the BEAST-A community teaching material resource for BEAST 2. Syst. Biol. 67, 170–174.

Bielejec, F., Baele, G., Vrancken, B., Suchard, M.A., Rambaut, A., Lemey, P., 2016. SpreaD3: interactive visualization of spatiotemporal history and trait evolutionary processes. Mol. Biol. Evol. 33, 2167–2169.

Briese, T., Calisher, C.H., Higgs, S., 2013. Viruses of the family Bunyaviridae: are all available isolates reassortants? Virology 446, 207–216.

Capobianchi, M.R., Castilletti, C., Gobbi, F.G., 2024. Potential risks of Oropouche virus importation into Europe. J. Trav. Med. 31, taae109.

Castilletti, C., Mori, A., Pomari, E., Matucci, A., Martelli, G., Curiale, S., Angheben, A., Gobbi, F.G., 2024. First diagnoses of Oropouche virus in Europe: how can we strengthen communication and preparedness globally? Lancet Infect. Dis. 24, e602–e603.

Cui, L., Liu, D., Shi, W., Pan, J., Qi, X., Li, X., Guo, X., Zhou, M., Li, W., Li, J., et al., 2014. Dynamic reassortments and genetic heterogeneity of the human-infecting influenza A (H7N9) virus. Nat. Commun. 5, 3142.

Deiana, M., Malago, S., Mori, A., Accordini, S., Matucci, A., Passarelli Mantovani, R., Gianesini, N., Huits, R., Piubelli, C., Gobbi, F.G., Capobianchi, M.R., Castilletti, C., 2024. Full genome characterization of the first Oropouche virus isolate imported in Europe from Cuba. Viruses 16, 1586.

Ding, Y.B., Guo, H.B., Hong, X.F., Li, Q.D., Miao, Z.J., Pan, Q.W., Zheng, K.Y., Wang, W. S., 2024. The distinct spatiotemporal evolutionary landscape of HBV and HDV largely determines the unique epidemic features of HDV globally. Mol. Phylogenet. Evol. 197, 108114.
Drummond, A., Pybus, O.G., Rambaut, A., 2003. Inference of viral evolutionary rates from molecular sequences. Adv. Parasitol. 54, 331–358.
Elbadry, M.A., Duraes-Carvalho, R., Blohm, G.M., Stephenson, C.J., Loeb, J.C., White, S. K., Telisma, T., Chavannes, S., Beau De Rochars, V.M., Salemi, M., Morris Jr., J.G., Lednicky, J.A., 2021. Orthobunyaviruses in the Caribbean: melao and oropouche virus infections in school children in Haiti in 2014. PLoS Neglected Trop. Dis. 15, e0009494.
Elliott, R.M., 2014. Orthobunyaviruses: recent genetic and structural insights. Nat. Rev. Microbiol. 12, 673–685.
Featherstone, L.A., Rambaut, A., Duchene, S., Wirth, W., 2024. Clockor2: inferring global and local strict molecular clocks using root-to-tip regression. Syst. Biol. 73, 623–628.
Gaillet, M., Pichard, C., Restrepo, J., Lavergne, A., Perez, L., Enfissi, A., Abboud, P., Lambert, Y., Ma, L., Monot, M., et al., 2021. Outbreak of oropouche virus in French Guiana. Emerg. Infect. Dis. 27, 2711–2714.
Graf, T., Delatorre, E., Do Nascimento Ferreira, C., Rossi, A., Santos, H.G.G., Pizzato, B. R., Nascimento, V., Souza, V., De Lima, G.B., Dezordi, F.Z., et al., 2024. Expansion of Oropouche virus in non-endemic Brazilian regions: analysis of genomic characterisation and ecological drivers. Lancet Infect. Dis. 25, 379–389.
Guagliardo, S.a.J., Connelly, C.R., Lyons, S., Martin, S.W., Sutter, R., Hughes, H.R., Brault, A.C., Lambert, A.J., Gould, C.V., Staples, J.E., 2024. Reemergence of Oropouche virus in the americas and risk for spread in the United States and its territories, 2024. Emerg. Infect. Dis. 30, 2241–2249.
Gunter, K., Omoga, D., Bowen, J.M., Gonzalez, L.R., Severt, S., Davis, M., Szymanski, M., Sandusky, G., Duprex, W.P., Tilston-Lunel, N.L., 2024. A reporter oropouche virus expressing ZsGreen from the M segment enables pathogenesis studies in mice. J. Virol. 98, e0089324.
Gutierrez, B., Wise, E.L., Pullan, S.T., Logue, C.H., Bowden, T.A., Escalera-Zamudio, M., Trueba, G., Nunes, M.R.T., Faria, N.R., Pybus, O.G., 2020. Evolutionary dynamics of Oropouche virus in South America. J. Virol. 94, e01127-19.
Harris, M., Caldwell, J.M., Mordecai, E.A., 2019. Climate drives spatial variation in Zika epidemics in Latin America. Proc. Biol. Sci. 286, 20191578.
He, W.T., Bollen, N., Xu, Y., Zhao, J., Dellicour, S., Yan, Z., Gong, W., Zhang, C., Zhang, L., Lu, M., Lai, A., Suchard, M.A., Ji, X., Tu, C., Lemey, P., Baele, G., Su, S., 2022. Phylogeography reveals Association between swine trade and the spread of porcine epidemic diarrhea virus in China and across the world. Mol. Biol. Evol. 39, msab364.
Hellert, J., Aebischer, A., Wernike, K., Haouz, A., Brocchi, E., Reiche, S., Guardado-Calvo, P., Beer, M., Rey, F.A., 2019. Orthobunyavirus spike architecture and recognition by neutralizing antibodies. Nat. Commun. 10, 879.
Ho, S.Y., Phillips, M.J., Cooper, A., Drummond, A.J., 2005. Time dependency of molecular rate estimates and systematic overestimation of recent divergence times. Mol. Biol. Evol. 22, 1561–1568.
Iani, F.C.D.M., Mota Pereira, F., De Oliveira, E.C., Nascimento Rodrigues, J.T., Hoffmann Machado, M., Fonseca, V., Ribeiro Adelino, T.E., Rocha Guimarães, N., Ribeiro Tomé, L.M., Astete Gómez, M.K., et al., 2024. Rapid viral expansion beyond the Amazon Basin: increased epidemic activity of Oropouche Virus across the americas. medRxiv. https://doi.org/10.1101/2024.08.02.24311415.
Katoh, K., Standley, D.M., 2013. MAFFT multiple sequence alignment software version 7: improvements in performance and usability. Mol. Biol. Evol. 30, 772–780.
Kocher, A., Papac, L., Barquera, R., Key, F.M., Spyrou, M.A., Hubler, R., Rohrlach, A.B., Aron, F., Stahl, R., Wissgott, A., et al., 2021. Ten millennia of hepatitis B virus evolution. Science 374, 182–188.
Korber, B., Myers, G., 1992. Signature pattern analysis: a method for assessing viral sequence relatedness. AIDS Res. Hum. Retrovir. 8, 1549–1560.
Ladner, J.T., Savji, N., Lofts, L., Travassos Da Rosa, A., Wiley, M.R., Gestole, M.C., Rosen, G.E., Guzman, H., Vasconcelos, P.F.C., Nunes, M.R.T., T, J.K., Lipkin, W.I., Tesh, R.B., Palacios, G., 2014. Genomic and phylogenetic characterization of viruses included in the Manzanilla and Oropouche species complexes of the genus Orthobunyavirus, family Bunyaviridae. J. Gen. Virol. 95, 1055–1066.
Lemey, P., Rambaut, A., Drummond, A.J., Suchard, M.A., 2009. Bayesian phylogeography finds its roots. PLoS Comput. Biol. 5, e1000520.
Lenharo, M., 2024. Mysterious Oropouche virus is spreading: what you should know. Nature. https://doi.org/10.1038/d41586-024-02746-2.
Martin, D.P., Murrell, B., Golden, M., Khoosal, A., Muhire, B., 2015. RDP4: detection and analysis of recombination patterns in virus genomes. Virus Evol. 1, vev003.
Martins-Filho, P.R., Carvalho, T.A., Dos Santos, C.A., 2024. Oropouche fever: reports of vertical transmission and deaths in Brazil. Lancet Infect. Dis. 24, e662–e663.
Mcdonald, S.M., Nelson, M.I., Turner, P.E., Patton, J.T., 2016. Reassortment in segmented RNA viruses: mechanisms and outcomes. Nat. Rev. Microbiol. 14, 448–460.
Mcgregor, B.L., Connelly, C.R., Kenney, J.L., 2021. Infection, dissemination, and transmission potential of north American Culex quinquefasciatus, Culex tarsalis, and culicoides sonorensis for Oropouche virus. Viruses 13, 226.
Membrebe, J.V., Suchard, M.A., Rambaut, A., Baele, G., Lemey, P., 2019. Bayesian inference of evolutionary histories under time-dependent substitution rates. Mol. Biol. Evol. 36, 1793–1803.
Minh, B.Q., Schmidt, H.A., Chernomor, O., Schrempf, D., Woodhams, M.D., Von Haeseler, A., Lanfear, R., 2020. IQ-TREE 2: new models and efficient methods for phylogenetic inference in the genomic era. Mol. Biol. Evol. 37, 1530–1534.
Moreira, F.R.R., Dutra, J.V.R., De Carvalho, A.H.B., Reis, C.R., Rios, J.S.H., Ribeiro, M.D., Arruda, M.B., Alvarez, P., Souza, R.P., Voloch, C., Zauli, D.a.G., Aguiar, R.S., 2024. Oropouche virus genomic surveillance in Brazil. Lancet Infect. Dis. 24, e664–e666.
Moutinho, S., 2024. Little-known virus surging in Latin America may harm fetuses. Science 385, 355.
Muller, N.F., Stolz, U., Dudas, G., Stadler, T., Vaughan, T.G., 2020. Bayesian inference of reassortment networks reveals fitness benefits of reassortment in human influenza viruses. Proc. Natl. Acad. Sci. U. S. A. 117, 17104–17111.
Nakase, T., Giovanetti, M., Obolski, U., Lourenço, J., 2023. Global transmission suitability maps for dengue virus transmitted by from 1981 to 2019. Sci. Data 10, 275.
Navarro, J.C., Giambalvo, D., Hernandez, R., Auguste, A.J., Tesh, R.B., Weaver, S.C., Montanez, H., Liria, J., Lima, A., Travassos Da Rosa, J.F., Da Silva, S.P., Vasconcelos, J.M., Oliveira, R., Vianez Jr., J.L., Nunes, M.R., 2016. Isolation of Madre de Dios Virus (Orthobunyavirus; Bunyaviridae), an Oropouche Virus Species Reassortant, from a Monkey in Venezuela. Am. J. Trop. Med. Hyg. 95, 328–338.
Naveca, F.G., Almeida, T.a.P., Souza, V., Nascimento, V., Silva, D., Nascimento, F., Mejia, M., Oliveira, Y.S., Rocha, L., Xavier, N., et al., 2024. Human outbreaks of a novel reassortant Oropouche virus in the Brazilian Amazon region. Nat. Med. 30, 3509–3521.
Naveca, F.G., Nascimento, V.A., Souza, V.C., De Figueiredo, R.M.P., 2018. Human Orthobunyavirus infections, Tefe, Amazonas, Brazil. PLoS Curr 10 ecurrents. outbreaks.7d65e5eb6ef75664da68905c5582f7f7.
Pan American Health Organization, W.H.O., 2024. Epidemiological Update: Oropouche in the Americas Region. PAHO/WHO, Washington, D.C.
Price, M.N., Dehal, P.S., Arkin, A.P., 2009. FastTree: computing large minimum evolution trees with profiles instead of a distance matrix. Mol. Biol. Evol. 26, 1641–1650.
Saeed, M.F., Wang, H., Suderman, M., Beasley, D.W., Travassos Da Rosa, A., Li, L., Shope, R.E., Tesh, R.B., Barrett, A.D., 2001. Jatobal virus is a reassortant containing the small RNA of Oropouche virus. Virus Res. 77, 25–30.
Sagulenko, P., Puller, V., Neher, R.A., 2018. TreeTime: Maximum-likelihood phylodynamic analysis. Virus Evol. 4, vex042.
Scachetti, G.C., Forato, J., Claro, I.M., Hua, X., Salgado, B.B., Vieira, A., Simeoni, C.L., Barbosa, A.R.C., Rosa, I.L., De Souza, G.F., et al., 2024. Re-emergence of Oropouche virus between 2023 and 2024 in Brazil: an observational epidemiological study. Lancet Infect. Dis. 25, 166–175.
Simon-Loriere, E., Holmes, E.C., 2011. Why do RNA viruses recombine? Nat. Rev. Microbiol. 9, 617–626.
Suchard, M.A., Lemey, P., Baele, G., Ayres, D.L., Drummond, A.J., Rambaut, A., 2018. Bayesian phylogenetic and phylodynamic data integration using BEAST 1.10. Virus Evol. 4, vey016.
Taylor, K.Y., Agu, I., Jose, I., Mantynen, S., Campbell, A.J., Mattson, C., Chou, T.W., Zhou, B., Gresham, D., Ghedin, E., Diaz Munoz, S.L., 2023. Influenza A virus reassortment is strain dependent. PLoS Pathog. 19, e1011155.
Tilston-Lunel, N.L., 2024. Oropouche virus: an emerging orthobunyavirus. J. Gen. Virol. 105, 002027.
Tilston-Lunel, N.L., Hughes, J., Acrani, G.O., Da Silva, D.E., Azevedo, R.S., Rodrigues, S. G., Vasconcelos, P.F., Nunes, M.R., Elliott, R.M., 2015. Genetic analysis of members of the species Oropouche virus and identification of a novel M segment sequence. J. Gen. Virol. 96, 1636–1650.
Travassos Da Rosa, J.F., De Souza, W.M., Pinheiro, F.P., Figueiredo, M.L., Cardoso, J.F., Acrani, G.O., Nunes, M.R.T., 2017. Oropouche virus: clinical, epidemiological, and molecular aspects of a neglected orthobunyavirus. Am. J. Trop. Med. Hyg. 96, 1019–1030.
Usuga, J., Limonta, D., Perez-Restrepo, L.S., Ciuoderis, K.A., Moreno, I., Arevalo, A., Vargas, V., Berg, M.G., Cloherty, G.A., Hernandez-Ortiz, J.P., Osorio, J.E., 2024. Co-Circulation of 2 Oropouche Virus Lineages, Amazon Basin, Colombia, 2024. Emerg. Infect. Dis. 30, 2375–2380.
Vasconcelos, H.B., Nunes, M.R., Casseb, L.M., Carvalho, V.L., Pinto Da Silva, E.V., Silva, M., Casseb, S.M., Vasconcelos, P.F., 2011. Molecular epidemiology of Oropouche virus, Brazil. Emerg. Infect. Dis. 17, 800–806.
Wesselmann, K.M., Postigo-Hidalgo, I., Pezzi, L., De Oliveira-Filho, E.F., Fischer, C., De Lamballerie, X., Drexler, J.F., 2024. Emergence of Oropouche fever in Latin America: a narrative review. Lancet Infect. Dis. 24, e439–e452.
Zhang, D., Gao, F.L., Jakovlic, I., Zou, H., Zhang, J., Li, W.X., Wang, G.T., 2020. PhyloSuite: an integrated and scalable desktop platform for streamlined molecular sequence data management and evolutionary phylogenetics studies. Molecular Ecology Resources 20, 348–355.